# Platinum electrochemistry through a magnifying glass

Jacobse, L.

# A EC-STM methods and general data processing

## A.1 Methods

The experiments described in Chapters 2-3 were carried out with the home-built EC-STM setup described previously.[1–3] This setup has proven to deliver high-resolution images, also on relatively rough surfaces, while still operating with significant scanning speeds. To allow for long-term experiments, for maintaining accurate control over the potentials, and for a high degree of cleanliness, we developed a new EC-STM cell with a reversible hydrogen reference electrode (RHE) that is compatible with the STM. A coiled platinum wire is used as counter electrode.

STM tips are electrochemically etched from $Pt_{80}Ir_{20}$ wire (Goodfellow) and coated with electrophoretic paint (Clearclad HSR) and polyethylene to minimize faradaic contributions to the tunneling current ($I_t$).[4] The Pt(111) sample (cut and polished <0.1°, Surface Preparation Laboratory, Zaandam, The Netherlands) is prepared by repeated cycles of mild etching (±2 V vs Pt, for 2.5 s at 50 Hz in an acidified $CaCl_2$ solution), flame annealing (5 min at ~1250 K), and cooling in a reducing atmosphere (1:4 $H_2$/Ar mixture). After the last cooling step, the surface is protected with ultrapure water (>18.2 MΩ·cm, Millipore Milli-Q) saturated with $H_2$/Ar. After each experiment the sample is sonicated in acetone to remove the black residue left by the Viton o-seal.

All parts of the electrochemical flow cell and the electrolyte reservoir are cleaned in freshly prepared piranha (3:1 v/v $H_2SO_4$ (Sigma-Aldrich, Puriss. p.a.) and $H_2O_2$ (Merck)) followed by at least five times boiling in ultrapure water. The tubing through which the electrolyte flows, is cleaned with a diluted piranha solution and extensively rinsed with ultrapure water. The 0.1 M $HClO_4$ electrolyte is prepared from high-purity perchloric acid (Merck suprapur) and purged with $N_2$ for at least 2 hours prior to the experiment.

Before starting the experiment, the surface quality and cleanliness was checked by (large scale) STM imaging and cyclic voltammetry. Under these conditions the sample potential ($U_s$) is not scanned above 0.85 V vs. RHE to prevent any change in the surface structure. Directly before and after each oxidation-reduction cycle, we

again record CVs up to 0.85 V to monitor the appearance of possible contaminants in between the oxidation experiments. All CVs are performed with the tip fully retracted (∼1 µm away) and at a fixed potential ($U_t$=0.45 V) to minimize the number of tip switches. Performing the ORCs with a retracted tip also prevents changes in the local sample potential due to the extremely small distance and large potential difference between the two electrodes. Such local potential changes would imply that the imaged area is no longer representative for the entire electrode surface. After each oxidation-reduction sequence (single ORCs for cycle 1-50, five ORCs for cycle 55-100, and ten ORCs for cycle 110-170) an STM image is acquired. During imaging the sample and tip potentials are fixed at $U_s$=0.4 V and $U_t$=0.45 V, respectively. This approach leads to a total data acquisition time of ∼17 hours. Unless mentioned otherwise, all data processing is performed with home-written routines using WaveMetrics Igor Pro software.

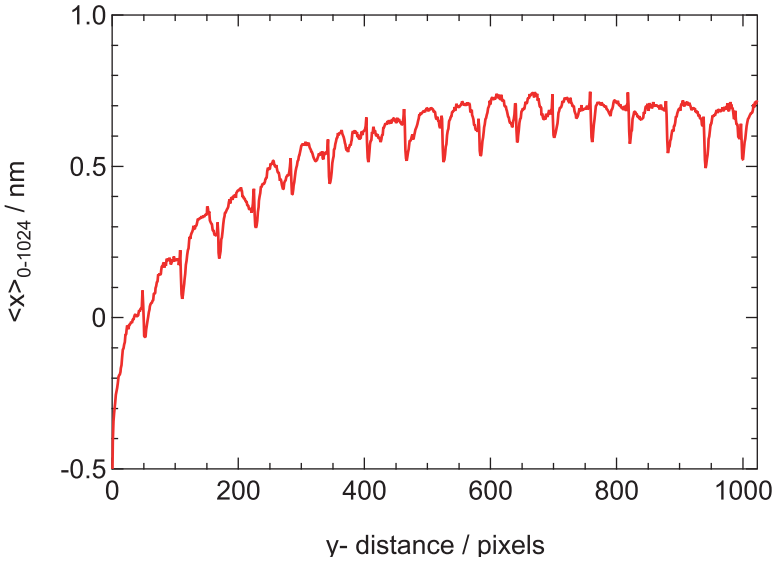


**Fig. A.1 | Distortion correction:** the average height along the x-direction, which is subtracted to correct for the creep and electrolyte flow distortions.

## A.2 EC-STM images

Our EC-STM data contain two distortions that need to be removed before applying a quantitative analysis. Firstly, as we retract the tip during the cyclic voltammetry, there is some creep in the z-direction which decays logarithmically along the slow scanning direction (y-direction). Furthermore, horizontal bands are observed in the images. The frequency of these bands corresponds to the frequency of the pump that regulates the electrolyte flow. As this behavior disappears over time, we attribute it to a faradaic current on the tip due to the presence of trace amounts of $O_2$. These distortions can be seen in the raw image which is shown in Fig. A.2A. Both distortions are removed by subtracting from each scan line (x-direction) the average value of that line. The magnitude of the correction is shown in Fig. A.1. After this correction, the sample tilt is removed by subtracting the best average fit of a plane through a single terrace. This results in the image that is shown in Fig. A.2B. Finally, in the analysis to determine site densities (Chapter 3), the image is corrected for the thermal drift, the result of which is shown in Fig. A.2C. Even though the thermal drift is small, it was found to have a small effect on the fitted nanoisland structures. The (time-dependent) drift vector is determined using cross-correlation functions on the whole set of images.

## A.3 Cyclic voltammetry

Our bipotentiostat and STM electronics operate separate from each other, but all the data is saved by the STM control software, and therefore perfectly aligned in time.[5] From these data we reconstruct cyclic voltammograms that are comparable to those measured with what is typically called 'current integration mode' for commercial (bi)potentiostats.

The charge related to hydrogen desorption is used as a measure for the number of available adsorption sites. This charge is determined by integrating the anodic current for sample potentials below 0.4 V after subtracting a (potential-independent) double layer current. Figure A.3 illustrates the determination of the hydrogen desorption charge for the pristine surface and after 8, 31, and 170 ORCs.

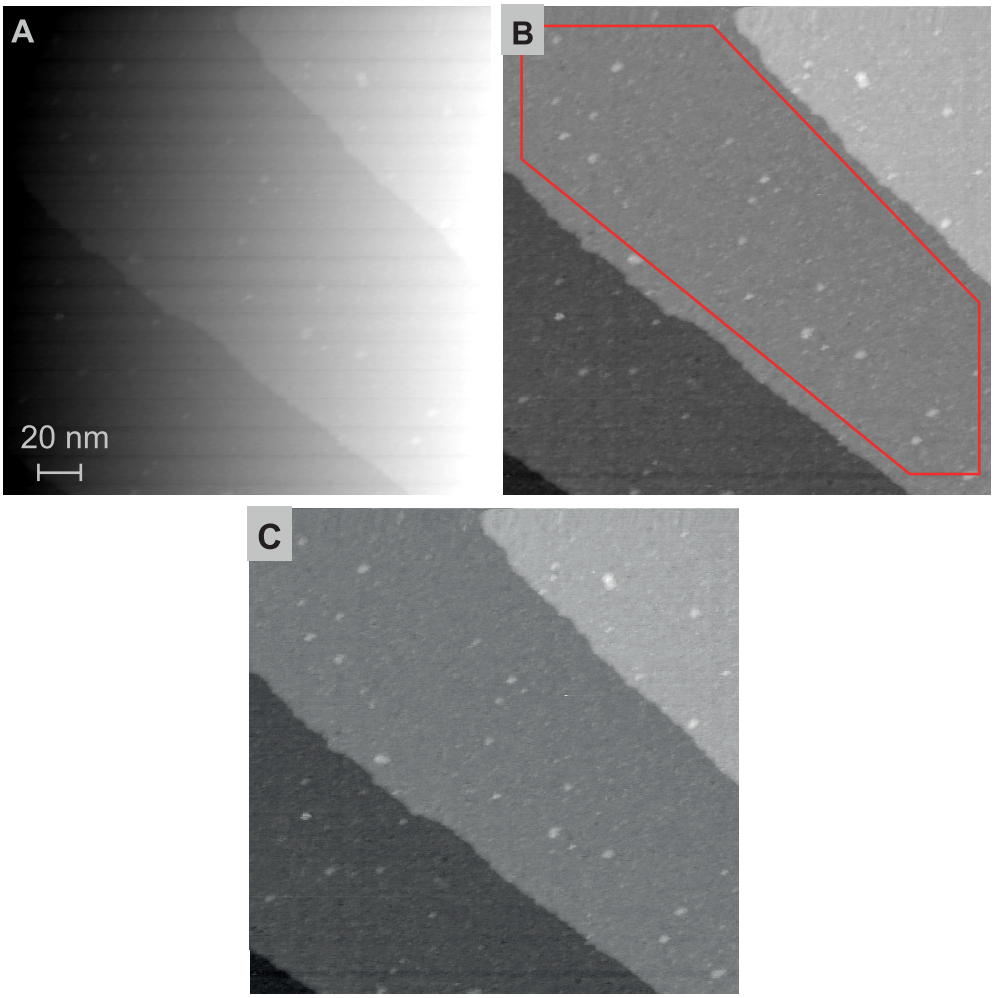


**Fig. A.2 | Image processing:** Panel **(A)** shows the raw EC-STM image of the pristine surface. **(B)** The same data after correcting for the distortions by creep, electrolyte pumping, and sample slope. The red line indicates the single terrace that is used for our analysis. **(C)** After applying the thermal drift correction.

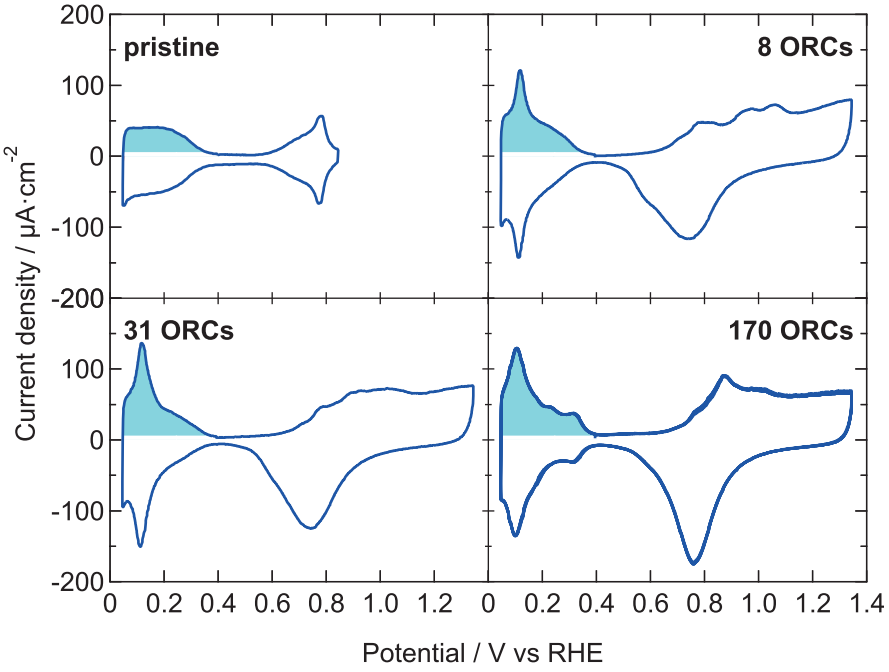


**Fig. A.3 | Hydrogen desorption charge determination:** the light blue areas indicate the charge related to the desorption of hydrogen for the pristine surface and after 8, 31, and 170 ORCs.

## References


1. Yanson, Y. I. & Rost, M. J. Structural Accelerating Effect of Chloride on Copper Electrodeposition. *Angew. Chemie Int. Ed.* **52,** 2454–2458 (2013).
2. Yanson, Y. I., Schenkel, F. & Rost, M. J. Design of a high-speed electrochemical scanning tunneling microscope. *Rev. Sci. Instrum.* **84,** 023702 (2013).
3. Rost, M. in *Encyclopedia of Interfacial Chemistry: Surface Science and Electrochemistry* 180–198 (Elsevier, 2018).
4. Güell, A. G., Díez-Pérez, I., Gorostiza, P. & Sanz, F. Preparation of reliable probes for electrochemical tunneling spectroscopy. *Anal. Chem.* **76,** 5218–5222 (2004).
5. Rost, M. J. *et al.* Scanning probe microscopes go video rate and beyond. *Rev. Sci. Instrum.* **76,** 053710 (2005).

# B Roughening analysis of Pt(111)

## B.1 Vacancy evolution

Remainders of the oxidation-reduction process could be an alternative explanation for the observation of the 'depressions' with a depth smaller than one monolayer. However, such 'residual oxides' should disappear over time, as they are thermodynamically unstable. Previously, the presence of 'residual oxides' was used to explain the increased reactivity of a Pt ultramicroelectrode towards the oxidation of hydrazine.[1] Thus activation already decreased significantly over the course of several minutes. Our oxidation-reduction cycles are separated by ~15 min., while we continuously record all signals. During this period we take three images. Figure B.1 shows one example of three subsequent images displaying the same part of the surface. During this set of images, the 'depressions' do not shrink and/or disappear. This static behavior makes it unlikely that the vacancy islands are actually 'residual oxides'.

## B.2 Scaling analysis

As stated in the main text, the three power law dependencies that should be evaluated to (dis)prove scaling are:

$$\begin{aligned} \xi_{\perp} &\sim t^{\beta} \\ \xi_{\parallel} &\sim t^{1/z} \sim t^{\beta/\alpha} \\ \xi_{\perp} &\sim \xi_{\parallel}^{\alpha} \end{aligned} \tag{B.1}$$

Scaling occurs when this analysis leads to consistent values for the scaling exponents ($\alpha$, $\beta$, and $z$). Although this analysis is typically performed for a continuous evolution in time (t), it was also demonstrated to be valid for situations where the evolution occurs in discrete steps (cycle numbers).[2] Figure B.2A to C show the results from the height-difference correlation analysis according to the power laws in Eq. B.1. Panel (A) shows the surface width as function of cycle number, (B) the parallel correlation length as function of cycle number, and (C) the surface width as function of parallel correlation length. These data are absolute values, whereas

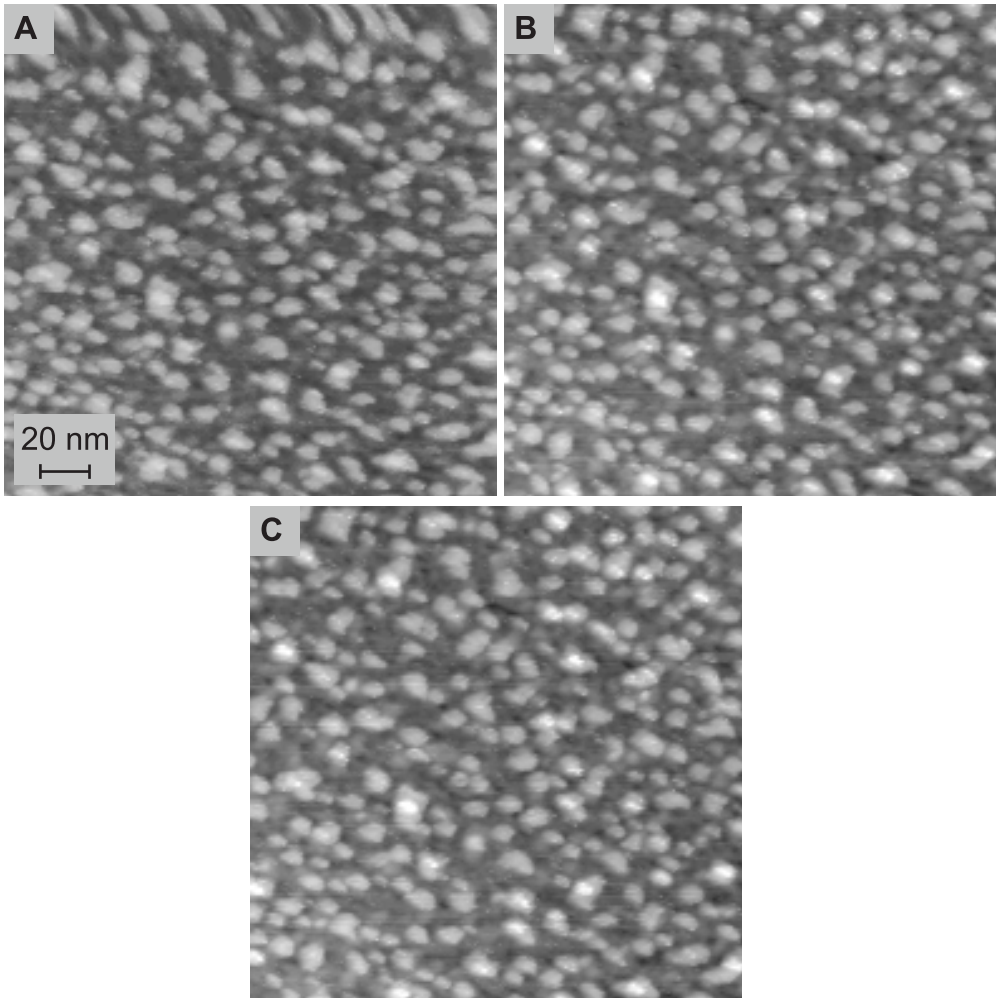


**Fig. B.1 | Time evolution of the vacancy islands:** three subsequent EC-STM images displaying the same area of the surface cropped to 100x100 $nm^2$. The time for recording all three images was ~15 min. During this time, the sample is kept at a constant, reducing potential ($U_s = 0.4$ V). These examples originate from a different set of data than those shown in the rest of the text.

values relative to the pristine surface would be necessary to determine the scaling exponents. However, this would lead to problems in panels (B) and (C) because most $\Delta\xi_{\parallel}$ would be negative as $\xi_{\parallel}(0) = 2.67$ nm. The value for $\beta$ shown in Fig. 2.5B ($\beta = 1.06 \pm 0.04$ during the first 15 ORCs, page 23) is determined after correcting for the offset of the perpendicular correlation length ($\Delta\xi_{\perp}(0) = 0.026$ nm) of the pristine surface. Nonetheless, the changing slope of the surface width indicates directly that scaling does not occur over the full range of 170 oxidation-reduction cycles (ORCs). This is expected as we distinguish two regimes: initially a 'nucleation & early growth' regime, which is followed by a 'late growth' regime. From the STM images and the correlation between the roughness and cyclic voltammetry, we argue that the transition between these regimes should occur between the 20$^{\text{th}}$ and 31$^{\text{st}}$ ORC. Scaling could still occur in each of these two regimes. However, the behavior of the parallel correlation length in the first 10 cycles (Fig. B.2B) demonstrates that scaling does not occur during the 'nucleation & early growth' regime.

Figure B.2D to F show the power law dependencies during the 'late growth' regime. The analysis of the correlation coefficient suggests that the 'late growth' regime starts ultimately at cycle 31. However, cycle 31-33 are omitted from the scaling analysis, as the values for $\xi_{\perp}$ strongly deviate from the power law dependence shown in Fig. B.2F. From the power law fits, we find $\alpha$=0.91 ± 0.09, $1/z$=0.54 ± 0.07, and $\beta$=0.69 ± 0.02. These values do not form a single consistent description according to Eq. B.1 and thus we have to conclude that scaling does also not occur in the 'late growth' regime between cycle 34 and 170. However, the ideal scaling exponents are only reached asymptotically when a transition is involved between two regimes. From Fig. B.2D it seems that $\beta$ decreases after ~75 ORCs ($\Delta$ cycle number = 41), whereas the other exponents remain constant. In this range we indeed find a smaller $\beta$ ($\beta_{75-170}$=0.62 ± 0.05), but due to the larger noise in $\xi_{\parallel}$ it is not possible to accurately determine $1/z$ and $\alpha$. Nonetheless, this observation suggests that scaling might be observed for even more extensive roughening experiments.

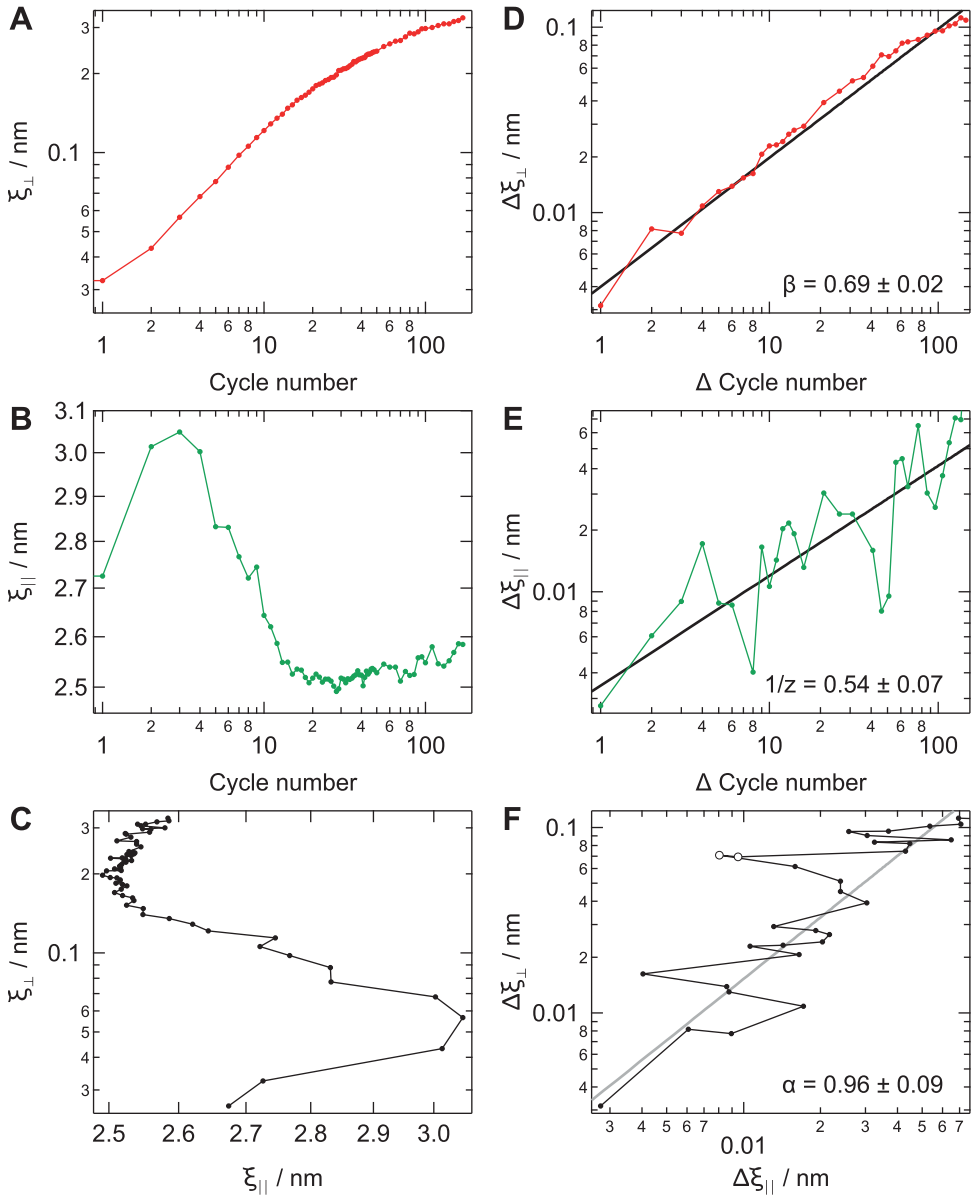


**Fig. B.2 | Roughness evolution during oxidation-reduction cycles:** **(A-C)** roughness evolution during all 170 ORCs. Panel B indicates directly that scaling does not occur. **(D-F)** roughness evolution during 'late growth' regime. The two values in (E) indicated with open symbols are considered outliers in the determination of $\alpha$. All values are relative to those determined after 34 oxidation-reduction cycles. Note that the (0,0) data point is not visible in this logarithmic plot. The straight lines are the power law fits to the data.

## B.3 Correlation coefficient

We define the cumulative correlation coefficient, quantifying the correlation between the hydrogen desorption charge and the surface width, as:

$$r(n) = \frac{\sum_{i=0}^{n}\left(q_{H,i} - \overline{q_{H,(0-n)}}\right)\left(\xi_{\perp,i} - \overline{\xi_{\perp,(0-n)}}\right)}{\sqrt{\sum_{i=0}^{n}\left(q_{H,i} - \overline{q_{H,(0-n)}}\right)^2} \cdot \sqrt{\sum_{i=0}^{n}\left(\xi_{\perp,i} - \overline{\xi_{\perp,(0-n)}}\right)^2}}, \tag{B.2}$$

in which $n$ is the cycle number. $\overline{q_{H,(0-n)}}$ and $\overline{\xi_{\perp,(0-n)}}$ are the mean hydrogen desorption charge and the mean surface width of the appropriate interval respectively. The validity of r(n) is determined by calculating its probable error as defined in the literature:[3]

$$probable\ error = \frac{0.6745(1-r^2)}{\sqrt{N}}, \tag{B.3}$$

where N is the number of data points taken into account.

## References


1. Aldous, L. & Compton, R. G. The mechanism of hydrazine electro-oxidation revealed by platinum microelectrodes: role of residual oxides. *Phys. Chem. Chem. Phys.* **13,** 5279–5287 (2011).
2. You, H. & Nagy, Z. Oxidation-reduction-induced roughening of platinum (111) surface. *Phys. B Condens. Matter* **198,** 187–194 (1994).
3. Eells, W. C. Formulas for Probable Errors of Coefficients of Correlation. *J. Am. Stat. Assoc.* **24,** 170–173 (1929).